Chemistry & Biology, Vol. 10, 1129–1137, November, 2003, ©2003 Elsevier Science Ltd. All rights reserved. DOI 10.1016/j.chembiol.2003.11.002

Nickel^{2+}-Mediated Assembly of an RNA-Amino Acid Complex

Sanchita Hati,[1] Amy R. Boles, John M. Zaborske, Brett Bergman, Amanda L. Posto, and Donald H. Burke*
Department of Chemistry
Indiana University
Bloomington, Indiana 47405

Summary

The RNA species SHR1 reacts with biocytin (ε-biotinoyl-L-lysine) in the presence of Ni^{2+} or Pt^{2+} to produce a metal-bridged complex that migrates more slowly than unreacted RNA in the presence of streptavidin (StrAv) on denaturing polyacrylamide gels. Mapping of reverse transcription pause sites identified G79 as a reactive nucleotide. G79 is near the 3′ end of a 37 nucleotide core motif that is nearly as reactive as SHR1. SHR1 reacts with biocytin in the presence of Pt^{2+} to yield a product that comigrates with the Ni^{2+} product but that is much more stable, suggesting that the metal ion used in the reaction is present in the product, possibly linking the RNA to the amino acid. In support of this model, SHR1 shows a strong affinity for Ni^{2+} in immobilized metal ion chromatography.

Introduction

The influence of metal ion availability and utilization on RNA function and evolution is important in the design of experiments to generate new RNA activities. Delimiting these influences is also important in understanding the range of activities that could have been available during an RNA world. Each metal ion provides a distinct combination of preferred coordination geometry, ionic radius, ligand exchangeability, charge density, and other properties that can be exploited by the RNA [1]. They can stabilize the close approach of phosphates in RNA secondary and tertiary structures through charge neutralization, and they can participate directly in catalytic reaction mechanisms. In addition to outer sphere coordination, the empty or partially filled *d* orbitals of transition metal ions potentiate inner sphere coordination with free ligands and with substituents of the RNA chain.

Natural ribozymes are all active in Mg^{2+}, as are most ribozymes derived from random sequence libraries. Mg^{2+}, Mn^{2+}, and some of the other metal ions most familiar to catalysis by ribozymes are generally hexacoordinate with octahedral geometry, while other divalent metals may prefer other coordination numbers and geometries. In vitro selections have expanded the range of metal ion preferences. One of the first of these was a self-cleaving RNA species known as the leadzyme, which uses Pb^{2+} in an autohydrolytic reaction [2]. A series of ribozymes that cap their 5′ ends with phosphorylated compounds [3–5] or with organic acids [6] all require Ca^{2+}. Some of the self-aminoacylating ribozymes require either Ca^{2+} alone or both Ca^{2+} and Mg^{2+} [7]. A self-cleaving deoxyribozyme (DNAzyme) uses Cu^{2+} as a redox-active center in the generation of peroxide radicals that cleave the backbone through Fenton-like reactions [8]. Amide-synthase [9] and Diels-Alderase [10] ribozymes carrying pyridine- or imidazole-modified uracils required Cu^{2+}. Wang et al. identified phosphoryl transfer DNAzymes with preferences for Mn^{2+}, Cu^{2+}, Mg^{2+}, or Zn^{2+} [11]. In most of these cases, neither the precise roles of the metal ions nor the reason for the observed metal ion specificity has been delineated, but these examples highlight the need for greater understanding of how metal ions influence the structure, function, and evolution of nucleic acids.

The availability of particular metal ions during in vitro selections for new catalytic or molecular recognition capabilities constrains the repertoire of RNA species that can be selected. If a given RNA species requires for high activity a metal ion that is not present in the reaction mixture, it will be rapidly eliminated from the library. Some selections therefore begin with an assortment of metal ions, deconvoluting individual metal ion requirements after the initial selection has been completed.

The present work sought RNA species that condense with a biotinylated amino acid, ostensibly as mimics of aminoacyl tRNA synthetases. Reaction products were captured on streptavidin (StrAv)-coated magnetic beads. Nine divalent metal ions were present during the selection: Mg^{2+}, Mn^{2+}, Ca^{2+}, Sr^{2+}, and Ba^{2+} in the millimolar to high-micromolar range, and Cu^{2+}, Co^{2+}, Ni^{2+}, and Zn^{2+} in the low-micromolar range. Surprisingly, the product formed by the selected RNA is noncovalent, forms independently of nucleotide cofactors, and is strictly dependent upon divalent nickel, for which the RNA shows marked affinity. The metal ion may serve as a bridge between the RNA and the amino acid. To our knowledge, this is the first published account of exclusive Ni^{2+} utilization by RNA and the first example of metal-bridged amino acid binding by structured RNA.

Results

Three Parallel Selections for Biocytin-Reactive RNA Species

Our initial objective was to produce a ribozyme that mimics the activity of aminoacyl-tRNA synthetases by first activating an amino acid at the expense of ATP hydrolysis, then transferring the amino acid onto its 3′ end. In selection 1, the RNA library was incubated with biocytin (ε-biotinoyl-L-lysine, Figure 1A) and ATP. In selection 2, 3′,5′-cyclic AMP (cAMP) was provided as an alternative energy source along with biocytin as substrate. In selection 3, RNA chains were initated with ATP rather than GTP through the use of a class II T7 RNA polymerase promoter. These RNAs were incubated with

*Correspondence: dhburke@indiana.edu
[1]Present address: Department of Chemistry, University of Minnesota, Minneapolis, Minnesota 55455.

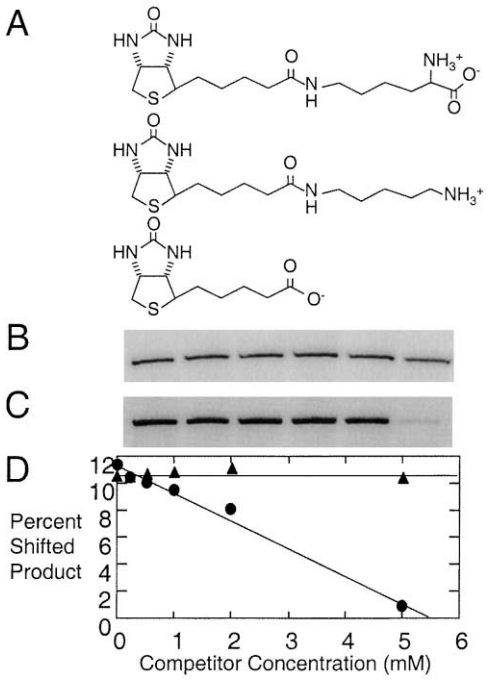

Figure 1. Substrate Utilization

(A) Structures of (top to bottom) biocytin, 5-(biotinamido) pentylamine, and biotin.

(B–D) Reactions of SHR1.48 with 5 mM biocytin in the presence of 0, 0.2, 0.5, 1, 2, or 5 mM biotin (gel B; triangles in [D]) or lysine (gel C; circles in [D]). Equal counts were loaded into each lane of the 10% denaturing polyacrylamide gels. Only product band is shown.

biocytin only. All three selections started from the same initial library, which included both random sequences and aptamer modules that had been preselected to bind ATP or biotin.

During each of the first seven cycles of the selection with ATP, approximately 0.25% of the input RNA was retained on the streptavidin (StrAv)-coated magnesphere beads, irrespective of the incubation time. The eighth and ninth cycles gave time-dependent signals, with 3% of the input RNA being retained after 18 hr at 4°C and substantially less at shorter times. The ninth round was repeated using a StrAv-dependent mobility shift on denaturing polyacrylamide gels to remove any undesired RNA species that may have copurified during the selection on StrAv beads. There was no further increase in product formation during two additional cycles on gels. Ribonuclease T1 digestion gave a uniform distribution of products for the early rounds where sequence complexity was high but gave nonuniform banding in the eighth round, indicating that one or a few sequences dominated the pool (data not shown). The population from the ninth round of selection 1 was converted to cDNA and cloned for sequencing. A single sequence, designated SHR1, appeared in all 20 isolates. This same sequence, with minor variations, also dominated isolates from round seven of selection 2 and from round ten of selection 3. Ten sequences unrelated to SHR1 formed no product under the conditions of the selection and appear to represent inactive species that had not yet been removed by the selection. Subsequent attention therefore centered on SHR1.

Substrate Specificity

Omission of a hydrolysable energy source, such as ATP or cAMP, had no discernable effect on product formation, nor did removing the 5′ triphosphate through treatment with alkaline phosphatase. In contrast, no mobility-shifted product was observed when biocytin was omitted from the reaction, nor when StrAv was omitted from the gel-loading buffer. Thus, biocytin is the only organic substrate required for product formation. No product is observed if biocytin is replaced with biotin or 5-(biotinamido) pentylamine. The former lacks the lysine portion of biocytin, while the latter lacks the lysyl carboxylate (Figure 1A). The carboxylate, and possibly the α-amino, of biocytin thus appear to be essential for its reaction with SHR1.

Stage-specific competition refined the basis of the biocytin requirement. Addition of free biotin at the beginning of the SHR1 reaction with biocytin did not affect product formation (Figures 1B and 1D); however, addition of free biotin after two sequential precipitations and prior to addition of StrAv for gel electrophoresis prevented the product from interacting with StrAv. Thus, the StrAv-dependent signal observed on gels and beads after product recovery is through the normal biotin-StrAv interaction. In contrast, free lysine significantly reduced product formation if added prior to the 18 hr reaction (Figures 1C and 1D) but had no effect if added along with StrAv after the 18 hr reaction. We conclude that lysine competes with biocytin, and that biocytinylation of the RNA during the 18 hr incubation depends upon interactions with the lysyl portion of biocytin. The degree of inhibition depends on the amount of lysine added. Product formation is largely eliminated when lysine is added at a concentration equal to that of the biocytin, suggesting that affinity to lysine may be greater than affinity to biocytin.

Product Formation Requires Divalent Nickel

No product was observed when Ni^{2+} was omitted from the reaction, but when Ni^{2+} was the only divalent ion present, up to 15% of the input RNA was shifted into the lower-mobility band (Figure 2A). This yield is nearly five times that observed during the selection, suggesting that one or more of the other metals may be inhibitory. Indeed, while several other divalent ions were tolerated, Mg^{2+}, Mn^{2+}, and Co^{2+} decreased reactivity when added at the same concentration as used during the selection (Figure 2B). Varying Ni^{2+} concentration from 0 to 10,000 μM gave maximal product formation at 8 μM, similar to the 10 μM used during the original selection (Figure 2C, diamonds). Higher concentrations inhibit the reaction, possibly due to nonspecific coordination with nucleobases that disfavor the reaction of SHR1 with biocytin (Figure 2C, inset). Elevated monovalent ion concentrations (>100 mM) weakly stimulated product formation, although Na^+, K^+, and Li^+ all gave equivalent reaction products. Thus, most subsequent reactions were carried out in 8 μM $NiCl_2$, 250 mM NaCl, and 50 mM PIPES (pH 7.0). The reaction appears to go to completion in

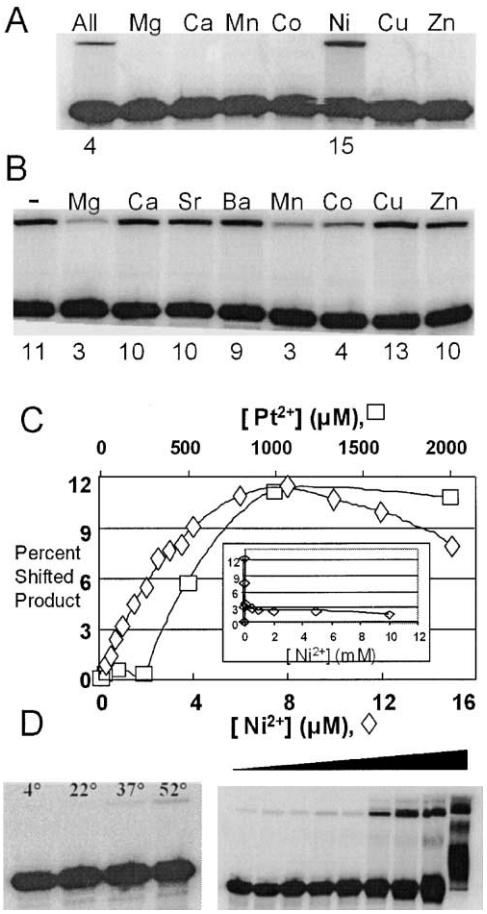

Figure 2. Divalent Metal Ion Requirements

(A) Reactions of SHR1 RNA with 5 mM biocytin in buffer A supplemented with the divalent ions listed above the lanes, each at the concentration used during the selection. Numbers below the lanes indicate the percentage of RNA in the low-mobility product band.

(B) Reactions were carried out in 10 μM Ni^{2+} supplemented with the ions shown.

(C) Plots of product yield between SHR1.48 and biocytin after 18 hr reactions at 4°C in the presence of Ni^{2+} (diamonds, scale below plot) or at 52°C in the presence of Pt^{2+} (squares, scale above plot). Inset shows percent RNA converted into product at higher Ni^{2+} concentrations.

(D) Reactions of SHR1.48 and biocytin in 10 μM Pt^{2+} after 18 hr at 4°C, 22°C, 37°C, and 52°C (left); and at 52°C in 0.01, 0.02, 0.05, 0.1, 0.25, 0.5, 1, 2, or 5 mM K_2PtCl_4 (right).

about 6 hr (data not shown), but overnight incubations were used throughout for ease of comparison.

Mapping the Site of Modification

To identify the functional RNA core, 29 different RNAs ranging in size from 29 to 118 nucleotides were transcribed in vitro and examined for their reactivity with biocytin in the presence of Ni^{2+}. Thirteen of these, including the original SHR1, formed low-mobility products with biocytin to varying extents. The 48 nucleotide SHR1.48 has a similar extent of reactivity as that of SHR1, while a 37 nucleotide core motif was nearly as reactive (Figure 3). Reverse transcription (RT) pause sites were mapped to determine the location of the modification. Unreacted SHR1 produced several pause sites, possibly due to interference from stable structures in the RNA. However, following overnight incubation with biocytin and Ni^{2+}, a new pause site appears with a 3′ end corresponding to C80 of SHR1, suggesting that a modification of G79 reduces efficiency of reverse transcription readthrough at that site (Figure 3A). An alternative interpretation would have the new pause site result from structural stabilization that reduces RT readthrough. However, as the nuclease digestion pattern (Figure 3C) is not altered following the reaction (data not shown), we conclude instead that G79 is modified in the Ni^{2+}-dependent reaction between RNA and biocytin.

Secondary Structure of a 37 Nucleotide Functional Core

The 37 nucleotide core is predicted to consist of three stems (S1 to S3) and two loops (Figure 3B). SHR1.48 RNA was subjected to enzymatic degradation analysis using ribonuclease V1 (specific for double-stranded RNA) and S1 (specific for single-stranded RNA). As expected, stems 1 and 2 are susceptible to V1 cleavage (Figure 4C). Similarly, loop 1 is strongly cleaved by nuclease S1. There appears to be a third stem, based on cleavage by nuclease V1 after U63/U64 and at G73 to A76. Several of the nucleotides in S3 are also cleaved by S1, however, so this stem may be in equilibrium with an open conformation. The V1 bands corresponding to S3 disappear when the probing is done at room temperature (data not shown).

Twenty-four site-specific mutations were made to test the mutability of SHR1.48. Extending stem 1—which contains the reactive site G79—to pair nucleotides 41–43 with nucleotides 81–83 increased product formation from around 12% to 18.5%. Truncated variants that remove a portion of stem S1 abolished product formation completely. Removing the reactive site G79 while maintaining structure by exchanging the C45–G79 pair for a G45–C79 pair abolished product formation. The remainder of SHR1.48 was also highly sensitive to mutation, as nearly every change introduced to the RNA abolished or significantly reduced formation of the shifted product. Notable among these inactive forms are (1) a mutant carrying an A52G/A57C pair to extend stem 2 into loop 2, (2) switching the strands of stem 2, and (3) a circular permutation with 5′ end at C55. (The complete set of mutants and their activities are available in the Supplemental Data online at http://www.chembiol.com/cgi/content/full/10/11/1129/DC1.) An all-DNA version of SHR1.48 was also inactive. Interestingly, all SHR1 variants isolated from the three selections were identical within the 37 nucleotide core, reinforcing the tight sequence constraints on this RNA. The reaction between SHR1, Ni^{2+}, and biocytin therefore results from a specific RNA structure—as opposed to representing a generic nucleic acid-nickel interaction—and is very sensitive to precise nucleotide sequence.

Evidence Against Formation of an Amide or Ester Linkage

Previous selection experiments have yielded RNAs that form aminoacylester, phosphoanhydride, or amide bonds

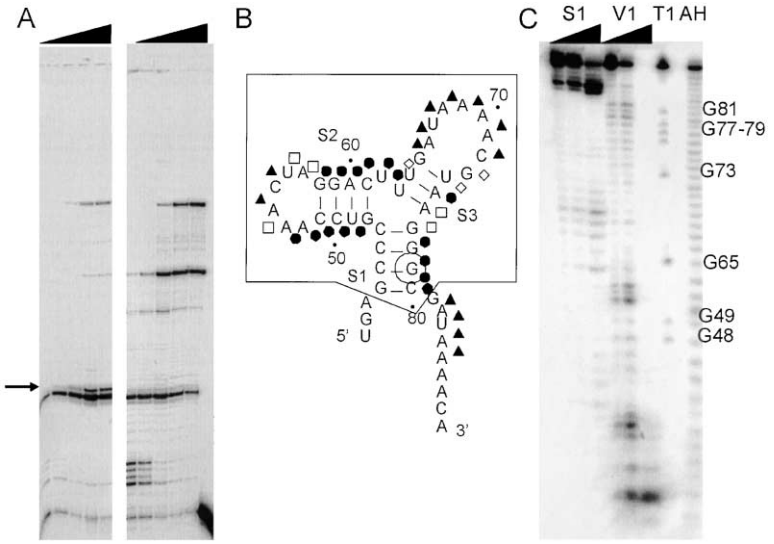

Figure 3. Secondary Structure of SHR1.48 RNA and RT Mapping of Modification Site

(A) Reverse transcription reactions were run for 0.5, 1.0, 5.0, 15, or 30 min on RNA that had been allowed to react with Ni^{2+} in the presence (left) or absence (right) of 5 mM biocytin. Arrow at left indicates the sole biocytin-dependent band, which maps to G79.

(B) Predicted core secondary structure of SHR1.48 RNA. Numbering is relative to parental SHR1 RNA (118 nucleotides). In addition to sequences shown, full-length SHR1 contains 5′ (CACGUUUGAACAUGUUU) and 3′ (UGACG) flanking sequences, as well as primer binding sites (see Experimental Procedures). Reactive site G79 is circled. The smallest active core motif, SHR1.37, is boxed. Cleavage sites for nucleases V1 (circles) and S1 (triangles) are indicated. Sites cleaved strongly by S1 and weakly by V1 are indicated by diamonds; sites cleaved strongly by V1 and weakly by S1 are indicated by squares. Numbering is as in full-length SHR1.

(C) Digestion of end-labeled SHR1.48 with S1, V1, or T1 nuclease, or by partial alkaline hydrolysis (AH). Numbering to the right is as relative to full-length SHR1.

with amino acids or organic acids. In each case, the amino acid was provided to the RNA in a preactivated form (aminoacyl adenylate, cyanomethyl ester, ribose ester, etc.), or the 5′ triphosphate of the RNA served as leaving group in the reaction (reviewed in [12]). None of these strategies is available to SHR1.48; thus, the reactions reported here are distinct from previously reported activities. Nevertheless, the observation of a mo-

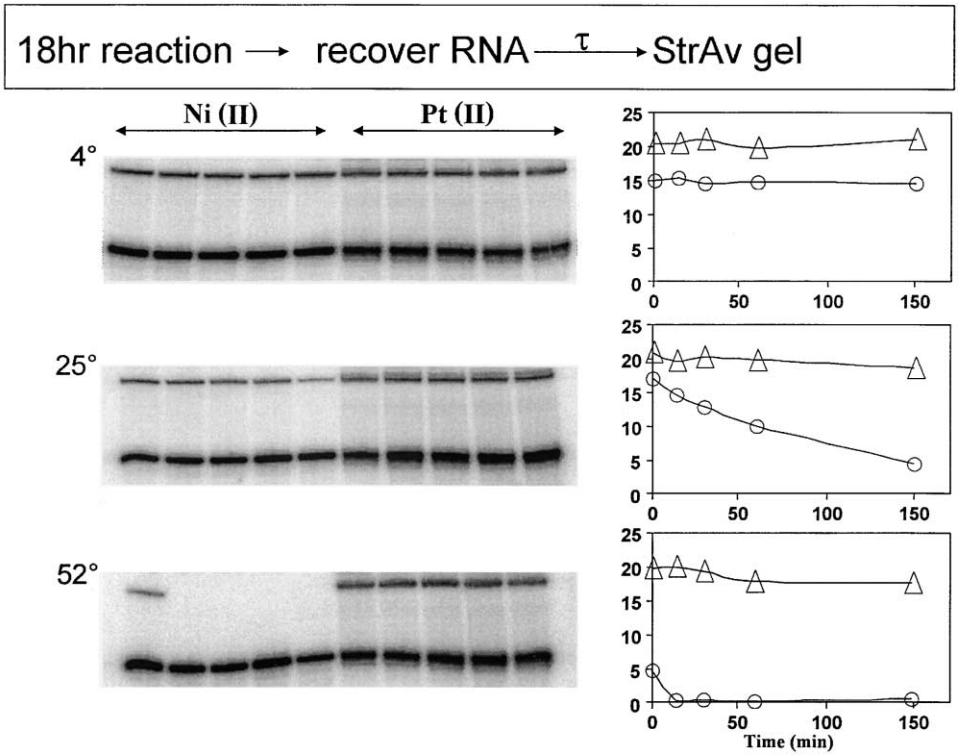

Figure 4. Product Stability

RNA SRH1.48 was incubated for 18 hr with biocytin in the presence of Ni^{2+} (left sides of gels, circles on plots) or Pt^{2+} (right sides of gels, triangles on plots), precipitated twice, then incubated in water for various times (τ)—1, 15, 30, 60, or 150 min—at the temperatures indicated before adding StrAv and separating by denaturing electrophoresis. Vertical axes on plots shows percent product in shifted bands.

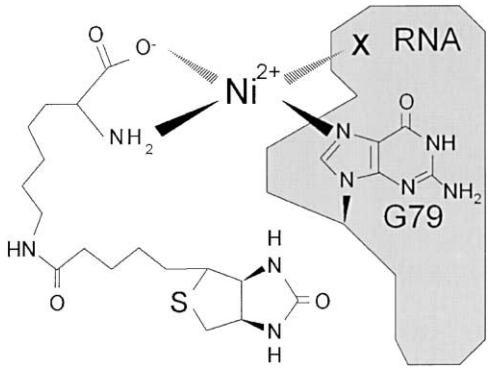

Figure 5. Model of RNA-Ni^{2+}-Amino Acid Interaction

Potential coordination geometry of Ni^{2+} coordinated with carboxylate and α-amino groups of biocytin, with the N7 of G79. A fourth ligand (X) could be a nitrogen or oxygen in the RNA—such as the N7 of G78—or a free water or chloride.

bility shift on denaturing gels containing EDTA begs the question of whether the amino acid is joined to the RNA through a newly formed covalent bond. Several approaches were used to investigate this possibility. First, when SHR1.48 was allowed to react with Ni^{2+} and biocytin, then digested to completion with P1 nuclease, and separated by either HPLC or thin-layer chromatography, peaks were observed only for the normal nucleotides. Second, none of the RNAs studied here produced a StrAv-independent mobility shift on acid gels, even though acid gels do allow the resolution of 2′(3′) aminoacylated RNA from unmodified RNA [13]. Third, matrix-assisted laser desorption ionization-time of flight mass spectrometry (MALDI-TOF MS) gave a sharp peak at the expected molecular mass for unreacted SHR1.37 but no new peaks following reaction with biocytin and Ni^{2+}. Thus, a direct RNA-biocytin covalent bond is not supported by methods capable of identifying ester- or amide-linked adducts.

Highly Stable Pt^{2+} Complex versus Unstable Ni^{2+} Complex

When 10 μM $NiCl_2$ was replaced with 10 μM $PdCl_2$ in reactions with 5 mM biocytin, a faint, StrAv-shifted product comigrates with the Ni^{2+}-derived product (data not shown). In the presence of 10 μM K_2PtCl_4, a water-soluble Pt^{2+} salt, no product was observed after 18 hr at 4°C. Platinum (II) complexes are kinetically more inert than nickel (II) and palladium (II) analogs [14], and the low temperature may not permit $PtCl_4^{2-}$ reactivity. Upon raising the temperature to 52°C, a faint but clearly discernable product band is formed (Figure 2D). On varying the concentration of Pt^{2+} from 10 μM to 5 mM, product yield increases to 12%–20% (Figures 2C and 2D). We have not examined in detail the apparently cooperative formation of the platinum-dependent product, although we caution that, as $PtCl_4^{2-}$ is the parent ion, the effective concentration of platinum may be significantly lower than the total concentration, yielding a falsely sigmoidal curve. The reactivity with nickel observed above thus also extends to additional metal ions (palladium and platinum) within the group VIII elements.

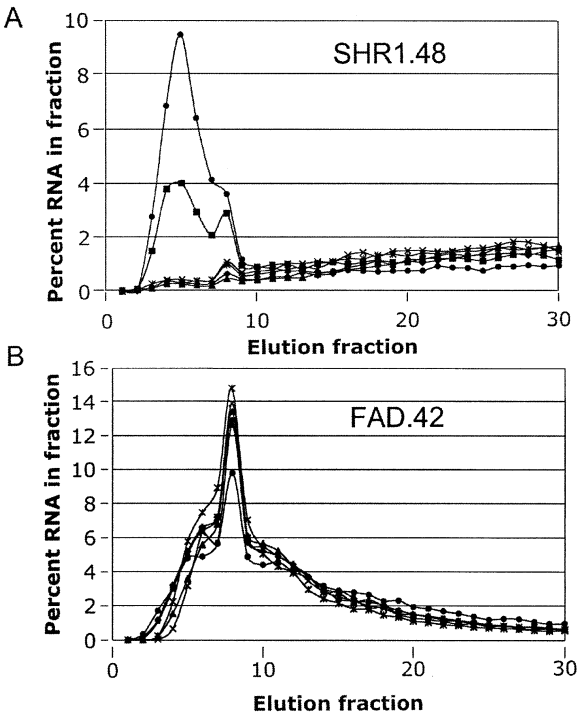

Figure 6. Immobilized Metal Ion Affinity Chromatography

Ni^{2+}-NTA colums were run with (A) SHR1.48 and (B) a 42-nucleotide FAD aptamer [15, 16]. Isocratic elutions contained Ni^{2+} at these concentrations: diamonds, 0; asterisks, 10 nM; triangles, 100 nM; X, 1 μM; squares, 10 μM; and circles, 100 μM.

Insight into the nature of the RNA-biocytin reaction began to emerge from a comparison of the stabilities of the products formed in Ni^{2+} versus Pt^{2+}. Both are mobility shifted by StrAv to comigrate on denaturing gels (Figure 4). The products from the reaction of SHR1 with biocytin and Ni^{2+} or with biocytin and Pt^{2+} are both stable for several hours on ice at pH 7.0. The same pair of reaction products show markedly different stabilities at higher temperatures. The product formed in Ni^{2+} degrades with an apparent half-life of approximately 1 hr at 25°C and less than 1 min at 52°C. In contrast, the product formed in Pt^{2+} degrades more slowly, with little decay at 25°C or 52°C over the course of several hours. For the metal ion used in the reaction to dictate stability of the product strongly suggests that the metal ion is still present in the product, with the metal ion bridging the RNA to the biocytin (e.g., Figure 5).

Direct Nickel Binding by SHR1 RNA

The possibility of a direct RNA-Ni^{2+} interaction was evaluated through immobilized metal ion affinity chromatography (IMAC). SHR1.48 was folded in NaCl and PIPES buffer along with varying concentrations of $NiCl_2$ then chromatographed isocratically over a Ni^{2+}-NTA resin equilibrated to the same buffer. Very little RNA eluted from the resin unless a high concentration (10 or 100 μM) of free Ni^{2+} was present (Figure 6A). In contrast, a control RNA of similar size selected to bind FAD [15, 16] eluted rapidly from the resin even when little or no free Ni^{2+} was present (Figure 6B). The retention of

SHR1.48 RNA on the Ni^{2+}-NTA resin suggests that SHR1.48 has greater affinity for direct binding to Ni^{2+} than that observed for an arbitrary control RNA, consistent with a direct, high-affinity metal ion-RNA interaction.

Discussion

Coordinate Complex with Ni^{2+}

While it is fairly common to include multiple divalent metal ions in selections for functional RNAs, most mixtures have not included Ni^{2+}. In a notable exception, Liu et al. identified a DNAzyme that cleaves RNA at very low pH in the presence of either Ni^{2+} or Mg^{2+} (other metals were not tested) [17]. Using IMAC, Hoffman et al. identified an RNA that binds to either Ni^{2+} or Co^{2+} through an unpaired purine-rich bulge [18]. Sigurdsson has shown that the hammerhead ribozyme is cleaved between G8 and A9 (not the canonical cleavage site) by Zn^{2+}, or, to a lesser degree, by Ni^{2+} or other ions [19]. While it is clear that nickel can serve useful roles in RNA chemistry, prior to the present work there have been no reports of any structured RNA that specifically utilizes Ni^{2+} to the exclusion of other first row transition metals.

Ni^{2+} ions coordinate with both oxygen and nitrogen donor atoms. They bind nucleosides and nucleotides predominately through N3 of pyrimidine bases and N7 or N1 of purine bases. For guanosine, the preferred binding site is N7 at pH 7.0, as the N1 is protonated at this pH (pKa, 9.2). For adenosine, both N1 and N7 are available to bind metal ions. Binding is quite weak, with stability constants (log K) for Ni^{2+} binding to nucleosides in the range of 0.3–1.4 [20]. At neutral pH, the affinities of a metal ion for specific binding sites of nucleobases in single-stranded nucleic acids follows the order N7G $>$ N3C $>$ N7A $>$ N1A $>$ N3A $\sim$ N3G [21]. Macrochelates can form when phosphate oxygen and purine N7 are coordinated simultaneously [20, 22]. Ni^{2+} also binds amino acids and peptides, forming complexes that are more stable than those with nucleotides (log K for lysine complex, 15.6 [23]). Binding is mainly through the carboxylate and α-amino groups. There are reports of ternary complexes of Ni^{2+}, amino acids, and nucleotides of stoichiometry [Ni^{2+}•(NTP)•(AA)•nH_2O] [24, 25].

Among the nine divalent cations available to the RNA during the initial selection (Mg^{2+}, Ca^{2+}, Ba^{2+}, Sr^{2+}, Mn^{2+}, Cu^{2+}, Co^{2+}, Ni^{2+}, and Zn^{2+}), only nickel supported the reaction, while Mg^{2+}, Mn^{2+}, and Co^{2+} were moderately inhibitory. Trace contaminant analysis by the manufacturer set upper limits for cobalt, copper, iron, and lead at 0.1%, 0.002%, 0.001%, and 0.0005%, respectively. As neither cobalt nor copper could replace nickel in the reaction, and as cobalt was notably inhibitory, trace contamination by these species could not contribute significantly to product formation. At the optimal 0.01 mM $NiCl_2$ concentration, iron or lead contaminant is expected to be less than 0.1 nM, versus 1–4 μM RNA. Thus, we ascribe the activity we observe to divalent nickel and not to contamination by trace metal ions.

The strict requirement for Ni^{2+} is quite unusual for RNA. Ni^{2+}, with a d^8 electronic configuration, can form complexes with variable coordination number and geometries. Hexacoordinate Ni^{2+} complexes are usually octahedral, similar to the preferred geometries for hexacoordinate Mg^{2+}, Mn^{2+}, and Co^{2+}. Trigonal bipyramidal and square pyramidal geometries are common for pentacoordinate complexes of Ni^{2+} and several other metals. For tetracoordinate complexes, square planar geometry is preferred over tetrahedral. The reverse preference is seen in tetracoordinate complexes of other first row transition metal ions Mn^{2+}, Fe^{2+}, Co^{2+}, Cu^{2+}, and Zn^{2+}, each of which prefers a tetrahedral geometry over square planar. Like Ni^{2+}, the second and third row transition metal ions Pd^{2+} and Pt^{2+} also have a d^8 electronic configuration, and their complexes are mainly square planar, although five-coordinate complexes are also known. This geometric preference for the tetracoordinate Ni^{2+} and Pt^{2+} ions to form square planar complexes is one feature that these metal ions share to the exclusion of the other divalent ions used in the selection and could conceivably account for the observed divalent metal ion preferences.

The product formed in the presence of Ni^{2+} decays rapidly upon mild heating, consistent with the weak binding of Ni^{2+} with the N7 of guanosine. Platinum belongs to the same chemical group as that of nickel, but its compounds are thermodynamically and kinetically more stable than nickel analogs. Like Ni^{2+}, Pt^{2+} interacts with amino acids and nucleotides and forms ternary complexes with nucleic acids and proteins. For example, the cytotoxic activity of cisplatin [*cis*-diaminedichloroplatinum (II)], a well-known square planar platinum complex used for the antitumor treatment of several malignancies, is due to the formation of DNA adducts, DNA-protein crosslinks, and both intrastrand and interstrand DNA crosslinks [26]. Incubating SHR1 with biocytin in the presence of $PtCl_4^{2-}$ yielded considerably more product when the reaction was carried out for 18 hr at 52°C than otherwise identical reactions at 4°C. The higher temperature may have accelerated the rate of reaction by mobilizing the kinetically inert Pt-Cl bonds of the $PtCl_4^{2-}$ salt. Kinetic inertness may also account for the higher concentration of $PtCl_4^{2-}$ required for optimal product formation (1 mM) versus that observed for Ni^{2+} (8 μM) and for the sigmoidal shape of the saturation curve. The product formed in the presence of Pt^{2+} remains intact at 25°C and 52°C for much longer than the SHR1-Ni^{2+}-biocytin product. We interpret this as evidence that the metal ion is present in the product as a coordinated SHR1-Pt^{2+}-biocytin complex.

Based on the observations above, we speculate that Ni^{2+} ions link SHR1 with biocytin to form a square planar, ternary complex. The Ni^{2+} may form coordinate covalent bonds with the α-amino and carboxylate groups of biocytin and with the N7 of G79. Additional contacts may be made with another guanosine (such as G78), with backbone phosphates, or with a water molecule (Figure 6). This model is supported by the RNA-Ni^{2+} affinity evidenced by immobilized metal ion chromatography. Alternative interaction models are possible but require additional assumptions that go beyond our data. For example, tight binding of nickel could facilitate biocytin binding at a secondary site. To preserve the potential for capture on StrAv, and to yield the competition observed in Figure 1, the RNA-biocytin interaction would

need to be primarily through the lysyl portion of biocytin and must somehow involve the amino acid carboxylate, which is shown to be required for product formation. The RNA-metal-amino acid complex we propose remains the most simple and straightforward and requires a minimum number of assumptions. We note that the apparent metal-bridged complex between the amino acid and the RNA could both position the amino acid and activate it for subsequent reactions.

The SHR1 sequence was isolated with minor variations from all three selections. While this may reflect independent, convergent isolations of the same structural motif, it is impossible to rule out the possibility that the apparent evolutionary convergence in fact resulted from trace crosscontamination of the pools. The RNA core is highly sensitive to sequence alterations, suggesting that a precise arrangement of the nucleotides is required for product formation with Ni^{2+} and biocytin. The smallest RNA molecule capable of forming the product is only 37 nucleotides, possibly making it suitable for detailed structural studies of the complex.

Prognosis for Metalloribozymes that Utilize Ni^{2+}

None of the known ribozymes prefers Ni^{2+}, in part because Ni^{2+} has not heretofore been routinely included in ribozyme or aptamer selection buffers. The functional roles observed for nickel in natural protein enzymes may foreshadow contributions of this metal to catalysis by nickel-dependent ribozymes that could arise in future selections. There are eight known classes of nickel-containing enzymes: urease, methyl-coenzyme M reductase (MCR), carbon monoxide dehydrogenase (CODH) and the associated acetyl-coenzyme A synthase (ACS), Ni-Fe hydrogenase, Ni-superoxide dismutase (NiSOD), glyoxalase I, and peptidyl-prolyl *cis/trans* isomerases (reviewed in [27, 28]). About half of these use Ni^{2+}, and about half use either Ni^{1+} or Ni^{3+}. The nickel atoms in these enzymes display a variety of oxidation states and coordination geometries. Moreover, the nickel ions are present as mono-, di-, and multinuclear centers. In most cases, the nickel serves either as a Lewis acid or as a redox-active center. The nickel ions can also form coordinate covalent bonds with substrates to facilitate catalysis. For example, the binuclear Ni^{2+} center in urease contains two Ni^{2+} ions in the active site bridged by a carbamylated lysine and a water molecule. One metal center is pentacoordinate (distorted square pyramidal geometry) while the other is hexacoordinate (octahedral) [29]. One Ni^{2+} ion acts as a Lewis acid by polarizing the carbonyl group of urea, and the second Ni^{2+} ion polarizes a water molecule for attack on the urea. In the redox-active center of MCR, mononuclear Ni^{2+} is first reduced to Ni^{1+}, which then catalyzes the redox reaction. Finally, nickel can be present in multinuclear centers, such as the redox-active [Ni-4Fe-5S] clusters in CODH. Thus, inclusion of Ni^{2+} along with other divalent metal ions could expand the functional repertoire of in vitro-selected RNA.

Significance

In vitro selections from random sequence libraries have identified a wealth of new RNA molecules that catalyze chemical transformations or that bind to specific ligands. While metal ions can generally augment RNA function by neutralizing negative charges, positioning and orienting ligands, acidifying water, and in other ways, the precise contributions of divalent ions to most of the newly selected RNAs has not yet been delimited. Variations from one metal ion species to another in ionic radius, covalent bond character, preferred coordination geometry, and other chemical properties can lead to marked metal ion preference by a given RNA.

The influence of metal ion availability on RNA function and evolution is important both in designing experiments to generate new RNA activities and in understanding the range of activities that could have been available during an RNA world. In the absence of foreknowledge as to which metal ion may be best suited to the goals of a given selection, a mixture of multiple divalent metal ions can be used in selections for functional RNAs. These mixtures have not routinely included divalent nickel. We report here the first account of exclusive Ni^{2+} utilization by an RNA. The RNA SHR1 forms a complex with biocytin (ε-biotinylated lysine) that absolutely depends upon Ni^{2+}, from among several other first-row transition metal ions.

Divalent nickel is used only sparingly in biology, but it is an indispensable component of several protein enzymes. The contributions of Ni^{2+} in those systems may foreshadow its roles in new RNAs that may be identified through the inclusion of Ni^{2+} in future selection experiments. For example, the apparent metal-bridged RNA-amino acid complex in SHR1 could both position the amino acid and activate it for subsequent reactions.

Experimental Procedures

Magnesphere beads, streptavidin (StrAv), and 5-(biotinamido)pentylamine were purchased from Pierce. DNA oligonucleotides were obtained from Integrated DNA Technologies (Coralville, IA). $NiCl_2$ was purchased from Mallinckrodt. Other chemicals were from Sigma. K_2PtCl_4 was used within 48 hr of preparation to avoid oligomerization of the platinum ions.

Pool Construction

RNA libraries were transcribed in vitro using T7 RNA polymerase (Epicentre Technologies, Madison, WI) in the presence of [α-^{32}P]UTP to yield 118 nucleotide transcripts of the form 5′-*gggaaaagcgaatca tacacaaga* (70x) *gggcataaggtatttaattccata*-3′, where "x" represents one of four sources of diversity. Half of the initial input RNA was transcribed from random-sequence templates, representing approximately 10^{14} different sequences. For one quarter of the initial input library, a 33 nucleotide, biotin binding pseudoknot aptamer isolated previously [30] was flanked by random-sequence segments of 16 and 21 nucleotides: 5′-(16N)GACCGTCAGAGGACACGGT TAAAAAGTCCTCTA(21N)-3′. The remaining quarter of the initial library contained ATP binding aptamer libraries derived from two different selections for aptamers to coenzyme A [31, 32]. ATP-initiated transcripts were synthesized from PCR products generated via a primer that replaced the normal class III promoter (GTP initiating) with a class II promoter (underlined): 5′-*AGTAATACGACTCAC TATTagggaaaagcg*...-3′ [33].

Selection Procedure

Each of three parallel selections was initiated with 12 nmol of gel-purified, uniformly radiolabeled RNA, distributed into 30 separate 100 μl reactions. At each time point in the second round, 800 pmols

RNA were used, and 400 pmols were used thereafter. For each 100 μl reaction, 400 pmols RNA in 60 μl water was unfolded at 75°C for 3 min. To initiate folding, 10 μl of 10× buffer A was added (1× buffer A = 150 mM NaCl, 50 mM LiCl, 50 mM KCl, 50 mM piperazine ethane sulfonate [PIPES] [pH 7.0]). After slow cooling in a thermocycler to 40°C, 10 μl of 10× buffer B was added (1× = 20 mM $MgCl_2$, 5 mM $CaCl_2$, 2.5 mM $MnCl_2$, 1 mM $SrCl_2$, 1 mM $BaCl_2$, and 10 μM each $CoCl_2$, $NiCl_2$, $CuCl_2$, and $ZnCl_2$). The mixtures were kept at 40°C for 11 min, lowered slowly to 20°C, then placed on ice for 5 min. Reactions were initiated by adding 10 μl each of biocytin and either ATP, cAMP (final concentration of 5 mM), or water. After 1, 3, or 18 hr at 4°C, reactions were moved to 20°C for 20 min, then quenched with 100 μl of stop solution (9 M urea, 0.6 M sodium acetate, 50 mM EDTA). We used 10 μg glycogen as a carrier to precipitate RNA with ethanol, in order to remove excess biocytin and metal ions. Pellets were resuspended without drying in 200 μl buffer C (1:1 mixture of AB buffer [containing 1× buffers A and B] and stop solution, pH 7.0), then precipitated a second time. Pellets were resuspended without drying in buffer C and loaded onto 600 μl StrAv-coated magnesphere beads (Pierce). After 5 min at room temperature, unbound RNA was removed by washing the beads four times with 6× SSC (1× SSC = 150 mM sodium chloride, 15 mM sodium citrate [pH 7.0]) and twice with 0.1× SSC. Beads containing captured RNA were resuspended in water with DNA primer 5′-tatggaattaaatacct tatgccc-3′, heated at 80°C for 2 min, then cooled to room temperature and reverse transcribed using 10 U MMLV reverse transcriptase (RT) (Epicentre Technologies) at 37°C for 1 hr. The cDNA in the supernatant from the beads from the 1, 3, and 18 hr time points were mixed, PCR amplified, and pooled to generate transcription template for the subsequent selection cycle.

Reactivity Screens and StrAv-Dependent Gel Mobility Shift Assay

Gel-purified RNA transcripts were desalted on Microcon YM10 molecular weight cutoff filters (Amicon) to remove residual EDTA and salts. This step was essential for consistent results when low concentrations of Ni^{2+} served as the only divalent ion in the reaction with 5 mM biocytin. Higher biocytin concentrations yielded less shifted product, apparently through competition for StrAv binding by residual biocytin. Reacted RNA was precipitated twice and resuspended without drying in 10 μl of a buffer containing 10 μM StrAv, 8 M urea, 25 mM PIPES, and 5 mM EDTA. After 5 min at room temperature, 10 μl of 2× gel-loading buffer was added (2× = 95% formamide, 10 mM EDTA, 0.1% bromophenol blue, 0.1% xylene cyanol). Samples were analyzed by electrophoresis at 4°C on a 10% denaturing polyacrylamide gel (19:1 acrylamide:bis) containing 7 M urea. Gels were dried and exposed to phosphor screens for analysis using ImageQuant software.

RT Mapping of Reactive Site G79

SHR1 RNA was folded as above and incubated with biocytin for 18 hr at 4°C in 1× buffer A and 10 μM Ni^{2+}, then ethanol precipitated twice. Modified RNA was captured on StrAv-coated magnesphere beads under denaturing conditions (4.5 M urea) and washed as above, then the beads were resuspended in MMLV RT buffer. Immobilized RNA was copied to cDNA in situ with 5 U MMLV RT and 5′ radiolabeled primer at 35°C. RNA was not heat denatured prior to addition of MMLV RT, to avoid thermal breakdown of biocytinylated product. At various time points, an aliquot of the reaction mixture was removed and quenched by heating at 90°C for 10 min in 0.1 M NaOH. Reaction mixtures were then neutralized, mixed with formamide-loading buffer, and analyzed by 15% denaturing gel electrophoresis.

Nuclease Probing of Secondary Structure

All enzymatic digestions were performed in 5 μL with 10 pmol of 5′ ^{32}P labeled RNA. Reactions with ribonuclease S1 (0.015–1.5 U, Promega) proceeded for 90 min at 4°C in 2 mM $ZnSO_4$, 15 mM sodium acetate, and 125 mM NaCl. Reactions with ribonuclease V1 (0.0025–25 U, Ambion) proceeded for 60 min at 4°C in the buffer supplied by manufacturer supplemented with 4 μg of yeast RNA. To generate size markers, reactions with ribonuclease T1 (0.0015–0.0015 U, cleaves 3′ to guanosines) were performed at 50°C for 10 min in 20 mM sodium citrate, 1 mM EDTA, 7 M urea, and 180 μg/ml tRNA. Partial alkaline hydrolysis ladders were generated by incubating the RNA for 90 s at 92°C in 40 mM NaOH and 2 mM EDTA. All reactions were quenched in 95% formamide-loading buffer and immediately cooled to −80°C until samples were loaded onto 10% denaturing polyacrylamide gels for analysis.

Analysis for Covalent Product

Radiolabeled SHR1.48 RNA (100 pmols) was incubated with 5 mM biocytin at 4°C for 18 hr and then precipitated twice to remove the excess biocytin. Pellets containing both reacted and unreacted RNA were digested with 5 U of ribonuclease P1, which cleaves RNA to mononucleotides, in 5 μl 10 mM sodium acetate (pH 5.2) at room temperature for 20 min. Cleaved products were chromatographed using cellulose-PEI thin layer chromatography with ammonium acetate solution in the mobile phase. The ammonium acetate was 100 mM when the radiolabel was in A, C, or U and 300 mM when the label was in G. For HPLC analysis, biocytin reaction products (2 nmoles) generated with SHR1.48 were digested with ribonuclease P1, passed through YM10 microcon filter to eliminate P1 enzyme, and separated on C8 reversed phase HPLC with a gradient of 100% ammonium acetate (100 mM, pH 5.2) to 50% ammonium acetate and 50% acetonitrile in 30 min.

Analysis for Nickel-Ion Affinity

RNA was unfolded in water at 75°C for 3 min, then cooled to room temperature and folded for 5 min in 250 mM NaCl, 50 mM PIPES (pH 7.0), supplemented with $NiCl_2$ at the indicated concentration, in a final volume of 100 μL. RNA was then moved to ice for 10–20 min before loading onto nickel-NTA resin. The resin was prepared by incubating 300 μl packed nickel-NTA resin with 150 μl water to form a pipetable slurry, to which 100 μl of 100 mM $NiCl_2$ was added to ensure that all chelation sites were occupied. The slurry was transferred to the column and drained, then washed with approximately 5 ml ice-cold water, followed by at least 2 ml of the same buffer used to fold the RNA. Folded RNA was then loaded onto the resin and washed isocratically with the same buffer in which it had been folded. Elution fractions were collected at 4°C every 100 μL, and RNA was detected by Cerenkov counting. Negative control RNA is a 42 nucleotide aptamer to FAD described previously [15, 16].

Acknowledgments

We thank John Gillece and Jay Kissel for technical assistance; and members of the Burke lab for critical comments on the manuscript. This material is based upon work supported by a Young Investigator Award from the Arnold and Mabel Beckman Foundation and by the National Science Foundation under grant MCB-9896363.

Received: August 12, 2003
Revised: September 3, 2003
Accepted: September 8, 2003
Published: November 21, 2003

References

1. Feig, A.L., and Uhlenbeck, O.C. (1998). The role of metal ions in RNA biochemistry. In The RNA World, Second Edition, R.F. Gesteland, T.R. Cech, and J.F. Atkins, eds. (Cold Spring Harbor, NY: Cold Spring Harbor Laboratory Press), pp. 287–319.
2. Pan, T., and Uhlenbeck, O.C. (1993). In vitro selection of RNAs that undergo autocatalytic cleavage with Pb^{2+}. Biochemistry *31*, 3887–3895.
3. Huang, F.Q., and Yarus, M. (1997). 5′-RNA self-capping from guanosine diphosphate. Biochemistry *36*, 6557–6563.
4. Huang, F., and Yarus, M. (1997). Versatile 5′ phosphoryl coupling of small and large molecules to an RNA. Proc. Natl. Acad. Sci. USA *94*, 8965–8969.
5. Huang, F., Yang, Z., and Yarus, M. (1998). RNA enzymes with two small-molecule substrates. Chem. Biol. *5*, 669–678.
6. Kumar, R., and Yarus, M. (2001). RNA-catalyzed amino acid activation. Biochemistry *40*, 6998–7004.
7. Illangasekare, M., Sanchez, G., Nickels, T., and Yarus, M. (1995).

Aminoacyl-RNA synthesis catalyzed by an RNA. Science *267*, 643–647.
8. Carmi, N., and Breaker, R.R. (2001). Characterization of a DNA-cleaving deoxyribozyme. Bioorg. Med. Chem. *9*, 2589–2600.
9. Wiegand, T.W., Janssen, R.C., and Eaton, B.E. (1997). Selection of RNA amide synthases. Chem. Biol. *4*, 675–683.
10. Tarasow, T.M., Tarasow, S.L., and Eaton, B.E. (1997). RNA-catalyzed carbon-carbon bond formation. Nature *389*, 54–57.
11. Wang, W., Billen, L.P., and Li, Y. (2002). Sequence diversity, metal specificity, and catalytic proficiency of metal-dependent phosphorylating DNA enzymes. Chem. Biol. *9*, 507–517.
12. Burke, D.H. (2003). RNA-catalyzed genetics. In The Genetic Code and the Origin of Life, L. Ribas de Pouplana, ed., in press.
13. Illangasekare, M., and Yarus, M. (1997). Small-molecule-substrate interactions with a self-aminoacylating ribozyme. J. Mol. Biol. *268*, 631–639.
14. Rau, T., and v Eldik, R. (1996). Mechanistic insight from kinetic studies on the interaction of model palladium (II) complexes with nucleic acid components. In Metal Ions in Biological Systems, H. Sigel and A. Sigel, eds. (New York and Basel: Marcel Dekker, Inc.), pp. 339–378.
15. Held, D.M., Greathouse, S.T., Agrawal, A., and Burke, D.H. (2003). Evolutionary landscapes for the acquisition of new ligand recognition by RNA aptamers. J. Mol. Evol. *57*, 299–308.
16. Roychowdhury-Saha, M., Lato, S.M., Shank, E.D., and Burke, D.H. (2002). RNA aptamers that bind FAD. Biochemistry *41*, 2492–2499.
17. Liu, Z., Mei, S.H., Brennan, J.D., and Li, Y. (2003). Assemblage of signaling DNA enzymes with intriguing metal-ion specificities and pH dependences. J. Am. Chem. Soc. *125*, 7539–7545.
18. Hofmann, H.P., Limmer, S., Hornung, V., and Sprinzl, M. (1997). Ni^{2+}-binding RNA motifs with an asymmetric purine-rich internal loop and a G-A base pair. RNA *3*, 1289–1300.
19. Markley, J.C., Godde, F., and Sigurdsson, S.T. (2001). Identification and characterization of a divalent metal ion-dependent cleavage site in the hammerhead ribozyme. Biochemistry *40*, 13849–13856.
20. Martin, R.B. (1988). Nickel ion binding to nucleosides and nucleotides. In Metal Ions in Biological Systems, H. Sigel and A. Sigel, eds. (New York and Basel: Marcel Dekker, Inc.), pp. 315–330.
21. Sabat, M. (1996). Ternary metal ion-nucleic acid base-protein complexes. In Metal Ions in Biological Systems (New York and Basel: Marcel Dekker, Inc.), pp. 521–555.
22. Mariam, Y.H., and Martin, R.B. (1979). Proximity of nucleic base and phosphate groups in metal ion complexes of adenine nucleotides. Inorg. Chem. Acta *35*, 23–28.
23. Brookes, G., and Pettit, L.D. (1976). Stability constants for complex formation between cobalt (II), nickel (II) and copper (II) and 2,3-diaminopropionic acid, 2,4-diaminobutyric acid, ornithine, lysine and arginine. J C S Dalton, 42–46.
24. Onoa, B., and Moren, V. (1998). Nickel (II) and copper (II) - L-cysteine, L-methionine, L-tryptophan-nucleotide ternary complexes. Transition Met. Chem. *23*, 485–490.
25. Molodkin, A.K., Esina, N.Y., and Tinaeva, N.K. (2002). Heteroligand nickel (II) and palladium (II) complexes with amino acids and ATP. Zhurnal Neorganicheskoi Khimii *47*, 953–955.
26. Chu, G. (1994). Cellular responses to cisplatin. The roles of DNA-binding proteins and DNA repair. J. Biol. Chem. *269*, 787–790.
27. Ermler, U., Grabarse, W., Shima, S., Goubeaud, M., and Thauer, R. (1998). Active sites of transition-metal enzymes with a focus on nickel. Curr. Opin. Struct. Biol. *8*, 749–758.
28. Watt, R., and Ludden, P. (1999). Nickel-binding proteins. Cell. Mol. Life Sci. *56*, 604–625.
29. Jabri, E., Carr, M., Hausinger, R., and Karplus, P. (1995). The crystal structure of urease from *Klebsiella aerogenes*. Science *268*, 998–1004.
30. Wilson, C., Nix, J., and Szostak, J. (1998). Functional requirements for specific ligand recognition by a biotin-binding RNA pseudoknot. Biochemistry *37*, 14410–14419.
31. Burke, D.H., and Hoffman, D.C. (1998). A novel acidophilic RNA motif that recognizes coenzyme A. Biochemistry *37*, 4653–4663.
32. Saran, D., Frank, J., and Burke, D.H. (2003). The tyranny of adenosine recognition among RNA aptamers to coenzyme A. BMC Evolution, in press.
33. Dunn, J., and Studier, F. (1983). Complete nucleotide sequence of bacteriophage T7 DNA and the locations of T7 genetic elements. J. Mol. Biol. *166*, 477–535.